Low-frequency relaxation modes and structural disorder in $KTa_{1-x}Nb_xO_3$

J. P. Sokoloff
Optical Sciences Center, University of Arizona, Tucson, Arizona 85721

L. L. Chase
Lawrence Livermore National Laboratories, Livermore, California 94550

L. A. Boatner
Oak Ridge National Laboratory, Oak Ridge, Tennessee 37830
(Received 12 July 1989)

A light-scattering study of the low-frequency excitations in single crystals of cubic and tetragonal $KTa_{1-x}Nb_xO_3$ ($x=0.26$ and 0.28) has been carried out by employing a technique which uses an Iodine filter to remove elastically scattered light. Low-frequency Raman and Fabry-Pérot components related to structural disorder in the mixed-crystal tantalate-niobate system were observed. The spectral shape, symmetry properties, and thermal behavior of these components are consistent with an eight-site order-disorder model of the sequence of structural phase transitions observed in ferrodistortive perovskites.

I. INTRODUCTION

Numerous investigations of phase transitions in the perovskite-structure, mixed-crystal system potassium tantalate-niobate ($KTa_{1-x}Nb_xO_3$, or KTN) have been carried out with the goal of accounting for the mechanisms responsible for the observed structural alterations. In the KTN solid-solution system, a multicritical point occurs at a niobium concentration corresponding to $x \cong 0.05$. Above this Nb concentration, KTN undergoes a cubic-tetragonal-orthorhombic-rhombohedral sequence of phase transitions where the various transition temperatures increase with increasing niobium concentration. This same series of phase transitions is also observed for both pure $KNbO_3$ and another ABO_3 oxidic perovskite, namely, $BaTiO_3$—a material for which there is also considerable controversy regarding the physical origins of the phase transitions. A number of investigations have produced results suggesting that the phase transitions in $BaTiO_3$ and $KNbO_3$ are not simply displacive but also have order-disorder character. Studies of the same type have also led to similar conclusions regarding the phase transitions in the KTN system. These studies have included early x-ray experiments[1,2] that gave structural indications of a "disorder type" sublattice and dielectric properties investigations in which the dielectric constant deviated from the Curie-Weiss law, thereby suggesting the presence of low-frequency ionic motion within a disordered sublattice.[3] Subsequently, the quasielastic-scattering features observed in Raman experiments[4,5] have provided additional evidence of dynamic disorder. More recently, experiments employing local probes such as NMR (Ref. 6) and extended x-ray-absorption fine structure[7] (EXAFS) have concluded that the Ta and Nb ions occupy off-center positions within the perovskite unit cell. Accordingly, there are structural, dielectric, bulk, and microscopic indications that the phase transitions in KTN have some intrinsic order-disorder character.

At temperatures well above the paraelectric-ferroelectric transition, KTN exhibits a "soft mode" that is generally characteristic of a nominally displacive phase transition. The temperature dependence of such "soft modes" has previously been treated using anharmonic lattice models of varying sophistication. In particular, in the case of $SrTiO_3$ (a material exhibiting a structural but nonferroelectric phase transition near 108 K) Bruce and Cowley[8] have described the soft mode by considering the temperature dependence of cubic and quartic Ti-O and Sr-O couplings. This approach has been further extended by Migoni *et al.*[9,10] who introduced temperature-dependent, higher-order, on-site core-shell constants for the oxygen ions into the model in a self-consistent manner. Subsequently, Kugel *et al.*[11] have applied a three-dimensional version of this latter model to account for the observed soft-mode frequency of KTN samples having a wide range of Nb concentrations. Their results have also been found to be consistent with both hyper-Raman spectra and second harmonic generation observed in cubic phase perovskites.[12,13] In the approach adopted by Kugel *et al.*, the soft mode frequency, which is very sensitive to the O-Ta and O-Nb coupling, is significantly altered by the nonlinear polarizability of the oxygen ions. This work asserts that it is the temperature dependence of the charge density deformation along the O-Ta and O-Nb chains that drives the paraelectric-ferroelectric phase transition in KTN. Kugel *et al.* have noted, however, that a mean field theory of this type is characterized by deficiencies in the vicinity of the phase transition—i.e., exactly in the region where the anomalous dielectric dispersion effects and central components in Raman scattering are most dramatic. Therefore, the success of the soft mode model in accounting for the observed soft mode frequencies and its consistency with the hyper-

Raman spectra and second-harmonic generation does not preclude the existence of additional dynamic effects such as relaxation modes that are prominent near the phase transition.

Soft modes and relaxation modes can be present simultaneously even at temperatures that are far removed from that of the phase transition. For example, central components have been observed in the Raman spectra of orthorhombic $KNbO_3$ (Refs. 14 and 15) and cubic and tetragonal $BaTiO_3$—materials with well-established soft modes in these phases. Central components have also been found in hyper-Raman (HR) scattering studies of KTN, $BaTiO_3$, and $KNbO_3$. These low-frequency modes have usually been interpreted as representing heavily damped or overdamped soft modes.[16–20] In one HR investigation of the low-frequency region in cubic $BaTiO_3$, however, a central component that was largest in the vicinity of the cubic-tetragonal transition temperature T_{c1} was interpreted as resulting from a soft phonon pseudospin coupling in which the pseudospin modelled the "flipping" of the Ti ion between three double minima of the ionic potential lying along the ⟨100⟩ directions.[21] Infrared reflectivity measurements have also been made near T_{c1}, which were completely consistent with a soft mode model. However, these measurements only extended down to about 30 cm^{-1}, i.e., well above the expected response region of any low-frequency disorder related modes.[22,23]

Raman scattering experiments in which an iodine filter is employed to remove the elastically scattered laser light represent a powerful approach to the study of low-energy excitations in solids. This experimental approach was recently used to investigate such excitations in both $BaTiO_3$ and $KNbO_3$.[14,15] For both of these systems, the observed low-frequency components exhibited symmetry, lineshape, and thermal properties that were consistent with an intrinsic eight-site, order-disorder model of the successive phase transitions. In the present work, the prior investigations are extended to the KTN system, and the results are also shown to be consistent with the eight-site order-disorder model.

II. EXPERIMENTAL METHODS AND RESULTS

In the KTN solid solution system, samples with relatively low concentrations of Nb have successive phase transitions that are so closely spaced in temperature that it is difficult to carry out a detailed study of any phase other than the cubic phase. Accordingly, the present investigations were performed using two KTN signal crystal samples with relatively high Nb concentrations, i.e., $x=0.26$ with $T_{c1}=246$ K and $T_{c2}=203$ K, and $x=0.28$ with $T_{c1}=252$ K and $T_{c2}=210$ K. KTN crystals with these compositions have relatively high cubic-tetragonal phase transition temperatures, and they remain in the tetragonal phase over a range of more that 40 K, thereby providing the opportunity to investigate a high-temperature phase other than the cubic phase.

The light scattering spectra were obtained using the 5145 Å line of an argon ion laser tuned to, and stabilized on, the absorption of an I_2 filter. By using this technique, the elastically scattered light could be essentially eliminated from the resulting spectra so that low-frequency features such as the central peak (CP) could be clearly observed. The additional structure introduced by the other absorption lines of the iodine filter is removed using a digital renormalization technique discussed elsewhere.[24] It should be noted, however, that this technique is somewhat limited for narrow features on the order of the spectrometer resolution, but larger than the separation of neighboring iodine absorption lines. All of the experiments were performed using a right angle scattering geometry, and the Raman quasielastic components were dispersed by either a double monochromator or by a triple-pass Fabry-Perot interferometer followed by a double monochromator.

The single crystal KTN samples investigated in this work were cut with ⟨100⟩ faces. Measurements were also performed using crystals with two pairs of ⟨110⟩ faces, but the results obtained were identical to those for samples with ⟨100⟩ faces, and therefore, they will not be reported here. Evaporated gold electrodes were used to apply a poling field of $\cong 5$ kV cm^{-1} along a ⟨001⟩ cube axis while the sample was cooled through the cubic-tetragonal transition. This procedure produced monodomain, tetragonal phase crystals. The resulting polar axis is denoted as Z, and the incident and scattered light propagates along the $X\langle 100\rangle$ and $Y\langle 010\rangle$ directions, respectively. The full scattering geometry is denoted $X(\varepsilon_i\varepsilon_s)Y$, where ε_i and ε_s are the polarizations of the incident and scattered light. In these experiments, either the $X(ZZ)Y$ geometry or the $X(ZX)Y$ geometry was employed. Because tetragonal KTN belongs to the point group C_{4v}, ZZ scattering measures A-symmetry excitations, which involve ionic motion parallel to the polar axis, and ZX scattering measures E-symmetry excitations, which involve ionic motion in a plane perpendicular to the polar axis.

Three measurements, which are discussed below, were made using these samples. First, Raman spectra ($\cong 1$ cm^{-1} resolution) provided information on both the low-frequency optic phonons and relatively broad quasielastic features. These data were presented elsewhere,[5] and will only be discussed briefly here. In a second measurement, which also utilized the Raman scattering configuration, the integrated intensity of the central features was recorded as a function of temperature. Here, the monochromator was positioned exactly on the laser line and set for a bandwidth of several cm^{-1}. The intensity of the light transmitted through the I_2 filter and monochromator was then monitored as a function of temperature. This intensity $I_{ij}(T)$ depended on the polarizer-analyzer combination $\varepsilon_i\varepsilon_j$, and in fact, the integrated intensity of both the E-symmetry and the A-symmetry central features, i.e., $I_{zx}(T)$ and $I_{zz}(T)$, could be obtained simultaneously by slowly sweeping the sample temperature ($\cong 0.6$ K/min) and rotating the analyzer by $\pi/2$ every 0.5 min. This approach insured that $I_{zx}(T)$ and $I_{zz}(T)$ were measured under identical conditions and eliminated the need for any relative normalization, except for that required to compensate for the different polarization efficiencies of the monochromator gratings. Finally, a

Fabry-Perot (FP) interferometer was used to study in detail the features within several cm^{-1} of the elastic line.

A. Raman spectroscopy results

Raman scattering experiments were only performed on the 28% Nb sample ($x=0.28$). The $X(ZX)Y$ spectra taken in the cubic phase above T_{c1} are shown in Fig. 1. These spectra show only a partially resolved Brillouin doublet plus some central components. The different intensities of the Brillouin components result from the incomplete correction of the I_2 filter attenuation for these very narrow features. At 300 K a broad central component with a full width at half maximum (FWHM) of about 50 cm^{-1} is observed for all polarizations of the incident and scattered light. As $T_{c1}=252$ K is approached, the CP narrows rapidly and grows in intensity. Below T_{c1} the CP persists, as can be seen in Fig. 2, which shows spectra taken using a monodomain sample with the $X(ZZ)Y$ scattering geometry. These spectra also contain a central component that is much narrower and more intense than the CP seen above T_{c1}. The "hard" (i.e., temperature independent) phonon at $\nu=200$ cm^{-1}, and labeled as the TO_2 mode in Fig. 2, is only Raman active in the tetragonal phase. Its appearance just below T_{c1} is an indication that the sample has gone through the cubic-tetragonal phase transition, and its narrow linewidth indicates that the sample is primarily monodomain. The broad band centered at 125 cm^{-1} in Fig. 2 is assigned to the A-symmetry component of the TO_1 mode, which corresponds to displacements of the Ta or Nb ions relative to the rigid oxygen octahedron. This TO_1 phonon response has a peak that moves to slightly higher frequencies below the phase transition, and this suggests that it is the A_1 component of the F_{1u} soft mode that is stabilizing just below the cubic-tetragonal transition. In contrast to the usual phonon population dependence on T, both the TO_1 and TO_2 phonon features increase slightly in intensity as the temperature is lowered and is due in part to the second-order nature of the phase transition. That is, the scattered intensity increases as the sample becomes more polar.

Figure 3 shows spectra taken in the $X(ZZ)Y$ scattering

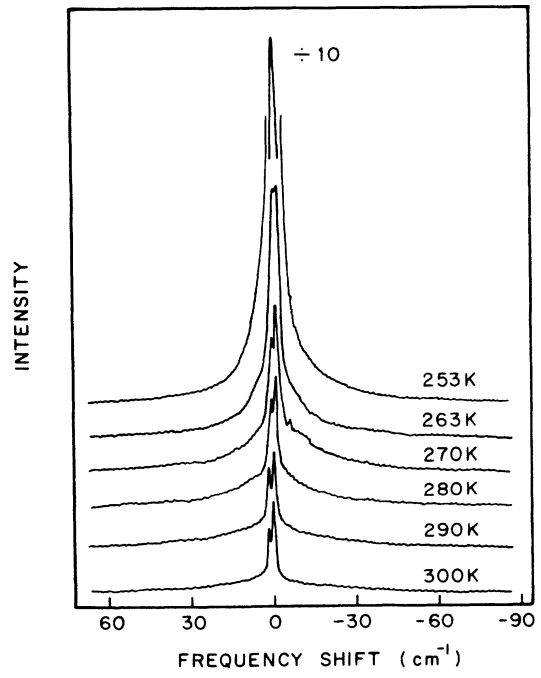

FIG. 1. Cubic phase Raman spectra showing the onset of the CP as the transition temperature is approached.

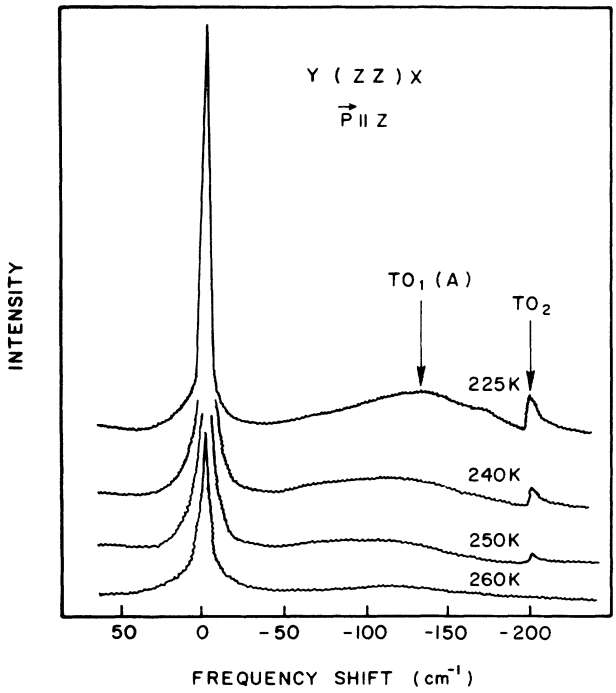

FIG. 2. Tetragonal phase A symmetry Raman spectra. The appearance of the TO_2 phonon indicates the crystal is a monodomain crystal in the tetragonal phase.

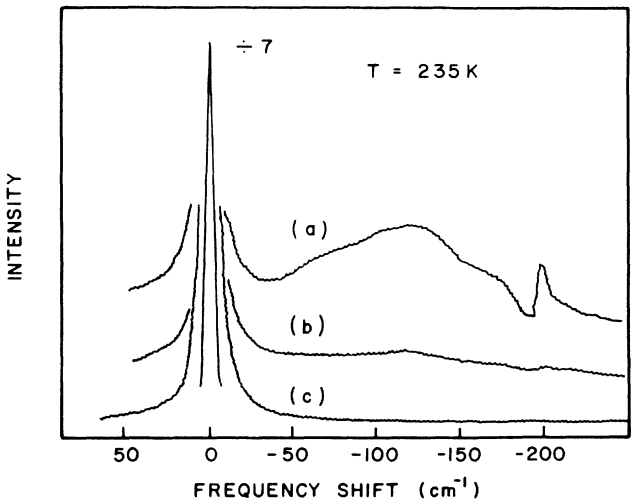

FIG. 3. Raman scattering at $T=235$ K: (a) $X(ZZ)Y$ spectra in a single domain; (b) $X(ZZ)Y$ spectra in an unpoled state; (c) $X(ZX)Y$ spectra in a single domain.

geometry well below the phase transition at $T=235$ K and illustrates the difference found when the sample is cooled through T_{c1} with [Fig. 3(a)] and without [Fig. 3(b)] an applied field. In the unpoled case of Fig. 3(b) both of the A-symmetry phonon features identified in Fig. 2 and present in Fig. 3(a) are nearly absent. Any domains that are present are evidently so small compared to the phonon wavelength (comparable to the laser wavelength) selected by the scattering geometry, that the spectrum is distributed over a broad range of wave vectors on the order of the reciprocal of the average domain size. These residual domains may be caused by perturbations such as random strains. Figure 3(c) shows an $X(ZX)Y$ spectrum from the monodomain sample. This spectrum is sensitive to E-symmetry excitations including those involving motion by the (Nb,Ta) ions perpendicular to the polar axis. The only feature present in this figure is an intense CP, and this apparently accounts for the entire spectrum of low-frequency E-symmetry excitations. Both the presence of this E-symmetry CP and the absence of the E component of the TO_1 phonon mode may represent evidence of dynamic disorder in the x-y plane. Furthermore, this E-symmetry CP is about a factor of 20 more intense than the A-symmetry CP at 225 K shown in Fig. 2, thus indicating that the tetragonal phase CP is primarily due to E-symmetry fluctuations.

In summary, the Raman scattering results for cubic phase KTN ($x=0.28$) show a CP that is extremely broad well above T_{c1} (FWHM$\cong$50 cm^{-1} at 300 K), but that narrows rapidly and increases in intensity as T_{c1} is approached from above ($T\rightarrow T_{c1}^{+}$). The fact that the CP changes so drastically as T approaches T_{c1} suggests that it is caused by structural disorder related to the onset of the phase transition. Below T_{c1} the CP persists and takes on definite polarization properties, displaying primarily E symmetry. Less intense CP is also seen in the scattering geometry sensitive to A-symmetry excitations, however, and it is not clear what fraction of the CP, if any at all, has A symmetry. To further investigate the relative symmetry contributions to the CP, measurements of the CP integrated intensity as a function of temperature [$I(T)$] were made. Unlike the CP's observed well above the phase transition, however, the shape of the CP's in the spectra taken at the lower temperatures are difficult to determine by means of Raman scattering because of their narrow width. In fact, the CP in each geometry may actually be composed of two or more components of different widths. In order to determine more accurately the lineshape of narrow components of the CP, the higher resolution scattering configuration, that employs a Fabry-Perot interferometer, was used. The results of these integrated intensity and Fabry-Perot measurements are discussed in the following sections.

B. Measurements of the CP integrated intensity

The integrated intensity measurement $I(T)$ described earlier is better suited to determining the relative intensities of the E- and A-symmetry CP at different temperatures. This method has the advantage that one experimental run provides information over a large temperature range. This minimizes normalization problems such as those caused by run-to-run changes in laser power, scattering regions, polarization geometries, or background contributions. The S-plane to P-plane efficiency of our monochromater, however, is about 1.3 so the $I_{zx}(T)$ intensity scale in our measurements should be interpreted as being 1.3 times larger than the $I_{zz}(T)$ intensity scale. The major disadvantage of this technique is that it integrates the CP intensity within a stationary frequency window. Therefore, if the width of a CP changes drastically, much of its intensity may only fall within this transmitted frequency range for a portion of a given temperature range. For example, at 300 K, well above T_{c1}, the CP has a FWHM of $\cong$50 cm^{-1}, and a monochromator output slit set to transmit only 1–2 cm^{-1} allows detection of only a very small portion of this CP. In the case of the KTN samples near and below T_{c1}, however, the CP has a much narrower width than at 300 K, and such a setting is sufficient to transmit most of the CP intensity. This gives a good indication of the relative weight of the E- and A-symmetry components of the CP—*particularly* within 1–2 cm^{-1} of the laser line. This is an important range because Raman spectra can provide any necessary information on the light scattered by more than a 1–2 cm^{-1} frequency shift.

Figures 4(a) and 4(b) show the integrated intensity of

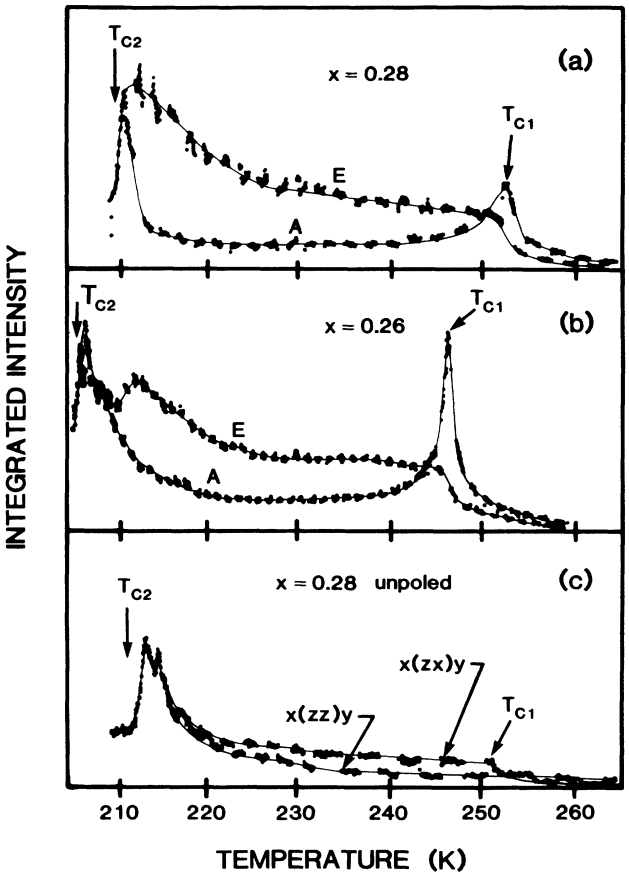

FIG. 4. Integrated intensity of the central peak as a function of temperature in KTN, for a bandwidth of 2 cm^{-1}, for (a) $x=0.28$ in a single domain; (b) $x=0.26$ in a single domain; (c) $x=0.28$ in an unpoled state. In these traces the data are represented by points, and the lines are a guide to the eye.

the CP for $x=0.28$ and $x=0.26$, respectively, obtained with the monochromator set for a bandwidth of 2 cm^{-1} and the sample poled and slowly cooled from a temperature of about $T_{c1}+30$ K. Both of the traces are qualitatively similar and clearly show that the A- and E-symmetry CP's have different integrated intensities. Although $I_{zz}(T)$ and $I_{zx}(T)$ both increase as T approaches T_{c1}^{+}, near T_{c1} the intensity $I_{zz}(T)$ increases more rapidly and displays a singularity at the phase transition. Below T_{c1}, $I_{zz}(T)$ decreases to a level that could be completely due to that part of the low-frequency tail of the $TO_1(A)$ mode which extends down to zero frequency shift. On the other hand, $I_{zx}(T)$ increases sharply but *smoothly* through T_{c1}, and then continues to slowly increase as the sample is further cooled. The qualitatively different and more dramatic behavior of $I_{zz}(T)$ at T_{c1}, as compared to $I_{zx}(T)$, is not surprising since it is the motion along the z axis (e.g., A-symmetry fluctuations) and not motion perpendicular to the polar axis, (e.g., E-symmetry fluctuations) that is most affected at a cubic-tetragonal phase transition. The gradual increase well below T_{c1} in both E and A traces could be due to a number of factors. The Fabry-Perot (FP) data in the next section, however, allow an unambiguous interpretation to be made of the integrated intensity data. When small changes were made in the width of the frequency bandpass or in the laser power, very little qualitative change was observed in the data for either polarization.

Figure 4(c) shows a trace taken when no electric field was applied to the sample. This "unpoled" data does not display polarization properties, and the scattered light is distributed fairly equally over both scattering geometries. These are the expected results for a polydomain sample that has no macroscopic scattering selection rules.

Based on the results of this section it can be concluded that the Raman data indicate that the CP in tetragonal KTN has E symmetry and that, additionally, a significant but narrow A-symmetry component of the CP is present in the vicinity of the phase transition.

C. FP spectroscopy results

The narrow central components in the KTN scattering spectrum were studied using the higher resolution provided by a FP interferometer with a free spectral range (FSR) of 172 GHz and a resolution of $\cong 2$ GHz (FWHM). These data provide complementary information to that obtained from the Raman scattering spectra and the integrated intensity measurements. The high resolution results establish that the low intensity, A-symmetry CP seen below the phase transition in the Raman scattering spectra is not simply an experimental artifact, and that no other sources beside the CP contribute to the measured $I_{zz}(T)$ and $I_{zx}(T)$ values. The Fabry-Perot measurements also show that the central components have an apparent Lorentzian lineshape centered on a zero-frequency shift that is indicative of a relaxation process.

KTN samples were examined under poled conditions in which an applied field induced a single domain tetragonal state as well as unpoled conditions where, below T_{c1}, translational ordering was present only on a small scale. Both KTN samples exhibited similar behavior below T_{c1}, but not above T_{c1}. Spectra from the 28% Nb sample were taken as a monodomain crystal and warmed through the tetragonal-cubic transition with the electric field applied. In this case some polarization effects were observed above T_{c1}, possibly because the applied field oriented tetragonal phase domains or precursor clusters which appeared just above the phase transition. Spectra from the 26% Nb sample were obtained as the crystal was cooled from a temperature of about $T_{c1}+10$ K through the transition with an applied field. Under these conditions, the spectra obtained at temperature above T_{c1} did not exhibit any detectable polarization properties. This result may be due to a hysteretic mechanism, such as random strains, which prevent the alignment of any precursor clusters or tetragonal phase domains already present in the crystal.

Figures 5(a) and 5(b) show the evolution of the CP as detected in the $X(ZZ)Y$ and $X(ZX)Y$ scattering geometry, respectively, for the monodomain 28% Nb KTN sample ($T_{c1}=252$ K). Below T_{c1}, the $X(ZX)Y$ data shown in Fig. 5(b), display an E-symmetry CP with a

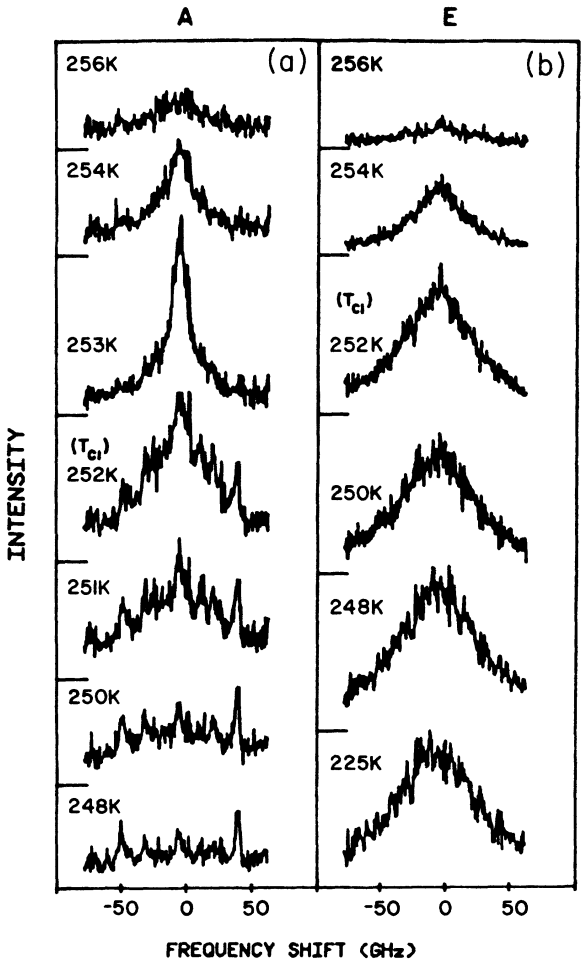

FIG. 5. FP spectra (a FSR of 172 GHz) for $x=0.26$ sample taken in the vicinity of T_{c1}: (a) $X(ZZ)Y$ spectra in a single domain; (b) $X(ZX)Y$ spectra in a single domain.

FWHM of $\cong 2.5-3.0$ cm^{-1} (75–90 GHz). This CP exhibits little change in either its width or intensity throughout the tetragonal phase, and therefore the increase in $I_{zx}(T)$ recorded in the integrated intensity measurements [see Figs. 4(a) and 4(b)] is not due to an increase in intensity of the E-symmetry CP. Above T_{c1} the E-symmetry CP seen in the $X(ZX)Y$ data retains the same basic shape as below T_{c1}, but its intensity is decreased.

The $X(ZZ)Y$ CP spectra [Fig. 5(a)] are much more temperature dependent than those taken in the $X(ZX)Y$ configuration. The $X(ZZ)Y$ spectra display features that are both narrow in width and increase in intensity significantly, as T_{c1} is approached from above, over a very small temperature range. Below T_{c1} however, these CP features quickly diminish in intensity. Since the features in this figure are due to scattering from polar domains or precursor clusters that presumably have their polar axes aligned with the polarizer and analyzer, they are assigned A symmetry—even above the phase transition. It is possible that a spectrum like that taken at $T=253$ K actually represents the sum of several CP's of different widths and scattering strengths, including a CP of only several GHz in width. In this case, however, the actual center of the spectrum would not be accurately reconstructed by the digital normalization technique, because a substantial part of the intensity would be absorbed by the iodine filter. Regardless of the composition of the $T=253$ K spectrum, however, a large portion of it has a width well within the $1-2$ cm^{-1} bandpass used in the collection of integrated intensity data, and it is this portion which is responsible for the singularity just above T_{c1} in the $I_{zz}(T)$ data.

As mentioned above the intensity of the CP features seen in the $X(ZZ)Y$ spectra falls off rapidly as $T_{c1}-T$ increases. In fact, several degrees below T_{c1} there is virtually no sign of any A-symmetry CP's of any width. It is worth noting that data taken using unpoled samples contained narrow CP features above T_{c1}, but, just as in the poled samples, they also disappeared below the phase transition. Therefore, if tetragonal ordering inhibits the fluctuations responsible for this narrow CP, then the ordered regions only have to be on the order of the size of a typical polar domain, as is the case in a polydomain sample.

III. DISCUSSION

The results presented in Sec. II show that above T_{c1} both E-symmetry and A-symmetry quasielastic scattering occur—the A-symmetry scattering being composed of possibly several CP's of considerably different widths. All of the CP's narrow and grow in intensity as $T\rightarrow T_{c1}^{+}$. Below T_{c1}, however, the E-symmetry CP persists and remains fairly constant in both width and intensity throughout the tetragonal phase. The A-symmetry CP's disappear, however, and this effect may be related to the tetragonal ordering along the polar axis of the crystal.

The characteristics of the observed central components may be understood in terms of an eight-site (ES) order-disorder model. A model of this type has been applied elsewhere to explain the central components and other anomalous light scattering features observed in the perovskite crystals, $BaTiO_3$ and $KNbO_3$.[14] In this model the B ion of the ABO_3 perovskite structure is located off-center in an eight-well potential that has each site (i.e., potential minimum) displaced from the unit cell center along a $\langle 111 \rangle$ direction. Such displacements may occur in isolated individual unit cells throughout the sample, or they may be correlated over certain regions in the sample. In either case, the different structural phases are a consequence of the preferential occupation of a certain set of sites by the B ions. For example, in the cubic phase the occupation of each of the eight sites would be the same. Below the first transition temperature preferential occupation of a set of four sites in a plane perpendicular to a particular axis would result in tetragonal ordering. The other phases are formed by a similar preferential occupation of yet another smaller subset of the eight sites that takes place at lower temperatures.

The ES order-disorder model also has a dynamic aspect. The height of the energy barriers separating the different sites affects the nature of the intersite and intrasite motion of the B ion, and therefore determines the spectral response of vibrational modes of the crystal involving the B ion. For instance, if the barrier between two equivalent sites is of such a magnitude that the B ion moves between these two sites in a periodic motion, then the ionic motion and spectral response $S(\nu)$ will be that of a damped phonon mode where

$$S(\nu)\propto \frac{\nu\Gamma}{(\nu_0^2-\nu^2)^2+\nu^2\Gamma^2} \ . \tag{1}$$

On the other hand, if the size of this barrier is such that interwell motion occurs at random times, then the motion is best described as a Debye relaxation. The spectral response will then be a Lorentzian centered on zero frequency shift with a HWHM approximately equal to the average B ion relaxation or "dwell" time τ, and $S(\nu)$ will be

$$S(\nu)\propto \frac{1}{1+\nu^2\tau^2} \ . \tag{2}$$

Another feature of this model is that, in the three ferroelectric phases, some of the eight sites of the local potential are energetically biased with respect to others due to macroscopic polarization within the crystal. In this case, the nature of the ionic motion between sites of different energy depends on the magnitude of the barrier height and potential bias. If these values are such that the B ion is largely confined to the low-energy well, then relaxation modes involving motion between inequivalent wells will be characterized by two dwell times that describe the average time spent by the ion in each potential well. The spectral response will correspondingly be composed of two Lorentzians with half widths at half maximum (HWHM) approximately equal to the inverse of the dwell times.

The present light scattering data for these KTN samples can be interpreted in terms of the eight-site model outlined above, and the results can be compared to those of a recent study of orthorhombic $KNbO_3$ and tetragonal

and cubic $BaTiO_3$, in which the same model was applied.[14] Below T_{c1}, KTN is in the tetragonal phase and the eight-site potential has fourfold symmetry about the polar axis. The top four sites in Fig. 6(a) (i.e., those in a plane perpendicular to the polar axis) have an identical occupation probability, as do the bottom four sites. One set of four sites, however, is preferentially occupied. The nature of the E-symmetry vibrational mode, in which the B ion moves perpendicularly to the polar axis among one set of four identical sites, is determined by the potential barrier between any two of these sites. In the case of tetragonal KTN, the barriers are much larger than the zero-point vibration energy of the B ion, and the B ion must either hop over or tunnel through the barrier to move from one well to another of the symmetric double-well potential (DWP). The time scale of such processes is longer than a typical optic mode period. This aspect is reflected in the low-frequency light scattering spectrum that is composed of the CP response, indicative of a relaxation mode, rather than the phonon response of a harmonic vibration. In contrast, in tetragonal $BaTiO_3$ and orthorhombic $KNbO_3$, the potential barrier between equivalent sites was comparable to the B-ion zero-point energy, thus accounting for both the low-frequency overdamped E-symmetry phonon in $BaTiO_3$ and the heavily damped B_2 phonon in orthorhombic $KNbO_3$.

The nature of the tetragonal A-symmetry vibrational mode is also determined by the barrier height and potential bias characterizing the asymmetric DWP's in which the B ion moves as it goes between two of the eight potential lying along a line parallel to the polar axis. In tetragonal $BaTiO_3$ (and orthorhombic $KNbO_3$) this motion was evidently relatively slow and the light scattering response contained two CP's each with a HWHM corresponding to the inverse of the average B-ion dwell time in either the upper or lower well of the asymmetric DWP. In tetragonal KTN, however, the potential barrier separating the two sites and/or the potential bias between the sites prohibits interwell motion polarized along the z axis. Accordingly, the A-symmetry spectra contain no CP. There is, however, a heavily damped phonon response present in the A-symmetry scattering spectrum, that was identified earlier as the $TO_1(A)$ mode. The sites involved in relaxation modes, as well as the local potential between two sites along the x (or y) and z axis, are shown in Figs. 6(a) and 6(b), respectively. In Fig. 6(b) E_0 is the zero-point vibrational energy of the B ion, V_0 is the potential barrier, and U is the potential difference along the z axis resulting from the macroscopic polarization within the crystal.

Above T_{c1} the presence of the central components can be explained as scattering from precursor clusters. The increase in scattered intensity as $T \rightarrow T_{c1}^{+}$ is due to either an increase in the number of precursor clusters and/or an increase in their average size. The idea that precursor clusters of a low-symmetry phase are present in the cubic phase has been discussed in connection with both $BaTiO_3$ and $KNbO_3$. There is also previous evidence in the case of KTN of precursor clusters (also referred to as ferroelectric microregions). This evidence is provided by Raman scattering studies,[5,24,25] and linear birefringence

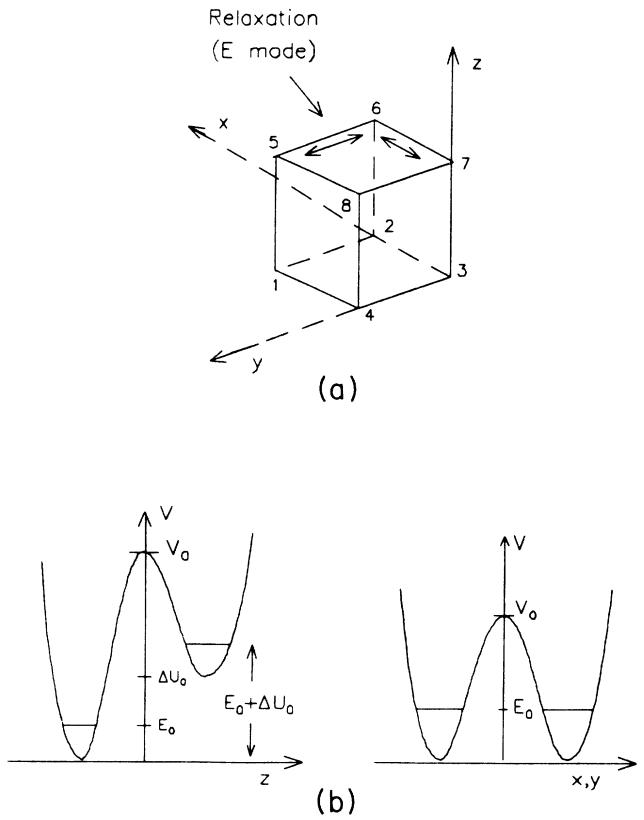

FIG. 6. (a) Low-frequency modes of motion of the Nb and/or Ta ion in tetragonal KTN. Motion in the x-y plane are E-symmetry relaxation modes; there are no interwell vibrational or relaxation modes polarized along the z axis. (b) The potential along a line between sites in the x-y plane, or parallel to the z axis.

and refractive index measurements.[26] As in the case of $BaTiO_3$, a particularly important question is whether the origin of the precursor clusters lies in an intrinsic or extrinsic mechanism such as coupling to impurities. Additionally, in the case of the mixed crystal KTN, the role of Nb ions in forming precursor clusters must be considered. A variety of models have been proposed to explain the polarization above T_{c1}, and these differ in their emphasis on the role of the defects as well as the characteristics of any short- or long-range order.

Various measurements[25,27,28] indicate that the dominant Nb displacement in a cluster is along a ⟨111⟩ direction, however, the origin of the off-center shift is a matter of controversy. While an intrinsic mechanism[29–31] may be responsible for this local region of lower symmetry, in most models it is impurity or defect related. An important distinction when discussing defects is the difference between symmetry-breaking (SB) and non-symmetry-breaking (NSB) defects.[32] Any substitutional defect breaks the translational symmetry of the lattice simply because it is different than the host atom it replaces; however, a SB defect also breaks the point group symmetry locally. The local dipole moment created by the off-center position of the SB defect can, in turn, polarize ad-

jacent defect-free unit cells. It is tempting to identify the isolated Nb ion, which is substituted for some Ta ions, as the defect resonsible for the clusters; however, isolated Nb may not be a SB defect. In fact, Prater *et al.*[33] studied several KTN samples with $x < 0.05$ and concluded that the "Nb ion is not a major contribution to the mechanism that breaks the lattice symmetry."

The evolution of the system from one which has only local order to one that displays long-range order is also described differently in the various phase transition models. The onset of long-range order depends on the nature of the interaction between the clusters. In one extreme, there is no long-range order; at low temperatures the system becomes a dipolar glass consisting of randomly oriented microdomains.[34] In another model,[26] the crystal is a "cooperative dipole glass" in which a strain-induced collective ordering of frozen-in microdomains occurs at the phase transition. Additionally, there is a model based on NMR data in which one Nb ion polarizes a "cloud" of about 100 Ta ions.[27] In this model orientational long-range ordering takes place because of an indirect coupling of these "clouds" via the host soft mode. Uwe *et al.*[24] have suggested that the size of a cluster is much smaller than 100 unit cells, but that it grows with decreasing temperature. In this model, the $KTaO_3$ host lattice contains ferroelectric microregions resulting from either very dilute randomly located polar defects of unknown composition or intrinsic fluctuations. In $KTaO_3$ these microregions vary from 1.3 unit cells in length at 100 K to 4.0 unit cells in length at lower temperatures. When the distorted regions begin to overlap, cooperative effects appear. Lyons *et al.*[25] have proposed a similar model except that the dipolar clusters surround a Nb ion and have a host-lattice correlation length that grows as the lattice softens. In this case there is a "delicate competition" near the transition between "tendencies toward long-range order and freezing in of a random cluster or glassy state;" however, the long-range order can be induced by the application of a strong electric field.[25] In the present studies, where approximately one in four Ta ions is replaced by a Nb ion, the average Nb-Nb separation is only two unit cells, and any cooperative effects need only have a very small interaction length. The model of Comes *et al.* proposed in 1968 for $BaTiO_3$ and $KNbO_3$ is an alternate description of a cluster.[35] In this model the crystal contains clusters in the form of chains of ions, all of which are displaced to equivalent off-center sites. Spectroscopic features such as CP's are then due to fluctuations in the site occupation of one or more of the ions in the chain. A similarity, however, between our results and those in Ref. 25 is that below T_{c1} long-range order occurs only if the sample is poled. Unless the sample is poled, it goes into a state below T_{c1} that is composed of tetragonal phase microdomains that are too small to exhibit optical phonons where wavelengths are comparable to that of the laser light. Internal fields of the microdomains, however, are large enough to prohibit A-symmetry fluctuations, as was indicated by the lack of any narrow central features in unpoled Raman data.

In summary, regardless of their exact origin or nature, regions of ferroelectric order are present in KTN above T_{c1}. Low-frequency fluctuations in these regions result in both E- and A-symmetry CP's. These CP's grow in intensity and narrow in width as $T \rightarrow T_{c1}^{+}$, reflecting a growth in the volume of precursor order and a decrease in the intersite relaxation rate of the B ions. Below T_{c1} there is sufficient polar order to supress A-symmetry fluctuations, even in unpoled samples. Dynamic disorder with E symmetry, however, persists throughout the tetragonal phase in the x-y plane. These features are all consistent with the eight-site model.

IV. ANALYSIS

The possibilities for a quantitative analysis of the KTN data are somewhat limited. Some quantitative checks of the accuracy of the eight-site model in describing KTN can be made, however. In particular, it is possible to determine if (1) the CP's, both above and below T_{c1}, have Lorentzian line shape centered on zero-frequency shift that is indicative of a Debye relaxation; (2) the widths of the CP's have the thermal dependence predicted by the ES model.

In order to check point (1) for the data taken above T_{c1}, the Raman data of Fig. 1 can be fit to the Debye relaxation response [Eq. (1)] in the region $-25 < \nu < 25$ cm^{-1}. A small region excluded from the fit (and indicated by the dashed lines in the $T = 280$ K trace) contains a Brillouin doublet and a narrow central peak that emerges between the doublet as $T \rightarrow T_{c1}^{+}$. Neither of these features have significant intensity for frequency shifts of more than a few cm^{-1} and should have a negligible effect on the fit. The fits to the data in Fig. 7 are adequate over the fitted regions and provide a measure of the intersite relaxation rate τ over a range of temperatures. A complete set of these τ values is listed in Table I. The narrow central component, which was well resolved in the high-resolution data, is also well fit by a Lorentzian. In particular, the $T = 253$ K trace in Fig. 5(a) had a FWHM of $\cong 12$ GHz; however, at higher temperatures this narrow component was not sufficiently intense to allow an accurate measurement.

Below T_{c1} it can be verified that the E-symmetry central component has a Lorentzian lineshape. Fits of the data in Fig. 5(b) to the spectral response of a Debye relaxation [Eq. (1)] are shown in Fig. 8, and these clearly provide a description of the fluctuations. Therefore, the CP's seen above T_{c1} in the Raman data, as well as the CP's seen both above and below T_{c1} in the FP data, have the line shapes associated with a relaxation mode.

Turning to point (2), it is possible to determine whether the relaxation times found by fitting the broad CP's in the Raman spectra are consistent with the ES model. To describe the relaxation mode more precisely, the tunneling model, which has been applied to dielectric data in tetragonal $BaTiO_3$, as well as spectroscopic data in cubic and tetragonal $BaTiO_3$ and orthorhombic $KNbO_3$, is used. In this semi-classical model[36] of phonon-assisted tunnelling, the thermally excited B ion tunnels through the top of a barrier confining it to a particular site or set of sites. The average dwell or relaxation time in this set of sites can be written

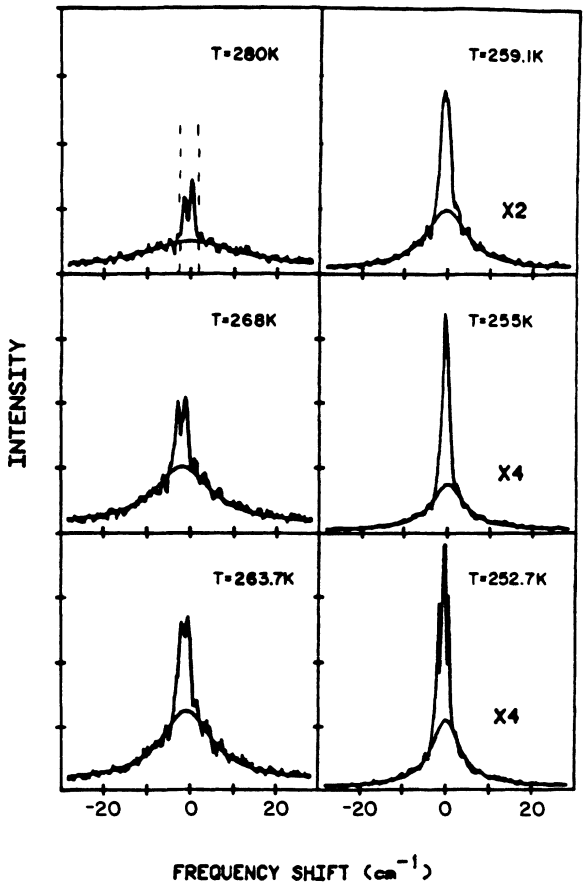

FIG. 7. Least-square fits of a Debye relaxation to the low-frequency cubic phase Raman data of Fig. (1). The region within the dashed lines in the $T=280$ K trace was not fitted in any of the data. The scaling factors indicate the magnitude of the fitted curve relative to the fitted curve in the $T=280$ K spectra.

$$\tau=\tau_0\exp\left[\frac{\Delta V-kT}{kT_0}\right] \tag{3}$$

Here $\Delta V=V_0-E$ is defined as the difference between the height of the barrier and the B-ion zero-point energy, $E=\langle E\rangle=kT$ is the average B ion additional thermal energy,

TABLE I. Values of τ resulting from a fit of the central peak in cubic KTN ($x=0.28$) to a Debye relaxation response, Eq. (3). The fits are shown in Fig. (7).

T (K)	$1/\tau$ (cm^{-1})	τ (10^{-12} s)
252.7	3.4	9.80
255	3.9	8.55
259.1	5.6	5.95
264	6.4	5.21
268	6.9	4.83
273	9.9	3.37
280	14.9	2.24
290	19.7	1.69
300	26.5	1.25

$$kT_0=\frac{\hbar}{2\pi}\sqrt{\alpha/m_B}$$

is related to the mass m_B of the B ion and the curvature α of the top of the potential barrier. The quantity $(\tau_0)^{-1}$ is a tunneling "attempt" frequency, and a typical physically plausible value for this quantity is several hundred cm^{-1}. This model differs from a hopping model in which the dwell time is described by an Arrhenius equation

$$\tau=\tau_0\exp\left[\frac{\Delta V}{kT}\right], \tag{4}$$

where ΔV is considered to be the activation energy of the B ion needed to hop from one well to another.

Either model can be applied to the CP spectra taken above T_{c1}, which are due to scattering from precursor clusters by making the assumption that any potential barriers and potential biases in a unit cell in a precursor cluster are temperature independent. Since the volume of precursor clusters in the sample is temperature depen-

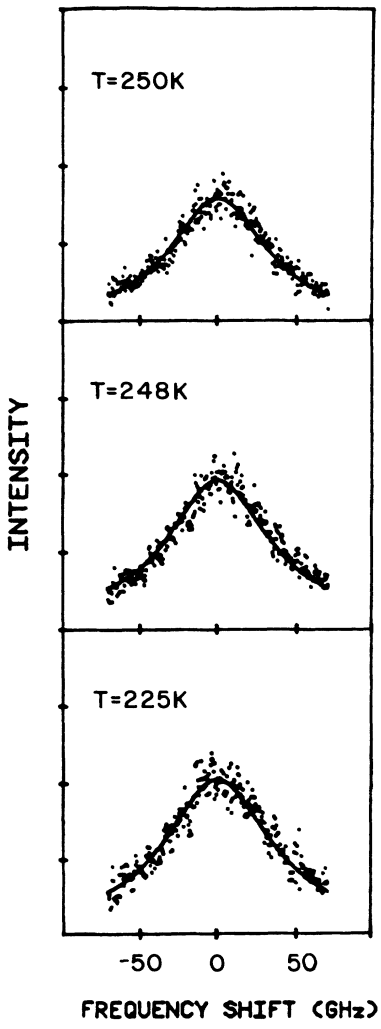

FIG. 8. Fit of the Debye response to the tetragonal phase E-symmetry FP spectra of Fig. 5(b). The data are the points; the fits are the lines. $\tau\cong 20\times 10^{-12}$ s for all three temperatures.

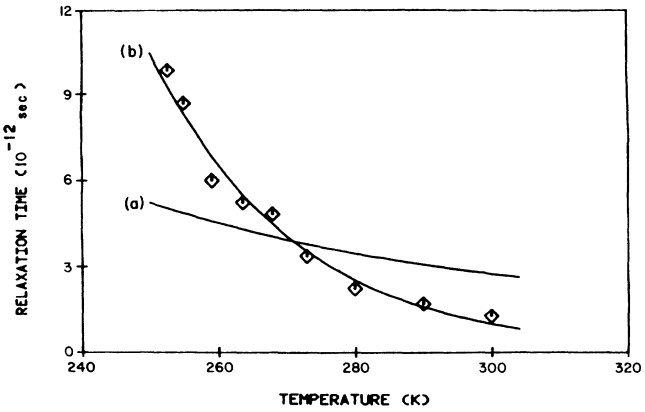

FIG. 9. Fit of relaxation times in Table I to the thermal behavior predicted by (a) the hopping model, i.e., $\tau=\tau_0\exp(\Delta V/kT)$, $1/\tau_0=300$ cm^{-1}, and $\Delta V=668$ cm^{-1}, and (b) the tunneling model, i.e., $\tau=\tau_0\exp[(\Delta V-kT)/kT_0]$, with $1/\tau_0=300$ cm^{-1}, $\Delta V=240$ cm^{-1}.

dent, the expected behavior of the integrated intensity is unknown. If the origin of the CP peak is either a single-particle hopping or tunneling mechanism, however, then the values of τ found from fits like those in Fig. 8 must be well fitted by either Eqs. 3 or 4. These two fits to the data are shown in Fig. 9. The hopping model apparently gives a poor fit while the tunneling model results in an excellent fit. This fit, in which a physically plausible attempt frequency of $1/\tau_0=300$ cm^{-1} was used, yields values of $\Delta V=240$ cm^{-1} and $kT_0=15$ cm^{-1}. A main assumption of this semiclassical tunneling model is that the Nb or Ta ion is thermally excited to near the top of the potential barrier and tunnels from that level to another potential site. Since the temperature $T=300$ K is equivalent to a thermal energy of 210 cm^{-1}, while $T_{c1}=252$ K is equivalent to 175 cm^{-1}, the value of $\Delta V=240$ cm^{-1} is consistent with the tunneling model for all of the Raman scattering spectra above T_{c1}. The value of kT_0 is a measure of the curvature of the center of the barrier α since, as defined earlier, $kT_0\sim\sqrt{\alpha}$. A small value of kT_0, such as $kT_0=15$ cm^{-1}, implies that the barrier width broadens rapidly below the top of the barrier. Therefore, small changes in a B ion's thermal excitation energy results in large changes in the size of the barrier width through which it must tunnel. This explains the strong temperature dependence of the relaxation time observed in the cubic phase.

In summary, both the shape and the width of the CP features seen in the Raman and FP spectra are quantitatively consistent with the version of the eight-site model used in the Sec. III to qualitatively describe the KTN spectra.

V. CONCLUSION

As for the other ferrodistortive ferroelectrics $KNbO_3$ and $BaTiO_3$, a relaxation mechanism is found to be present in KTN. A model in which the central ion of the perovskite unit cell tunnels among the different sites of an eight-site potential was used to describe this process. This eight-site model was tested in an earlier paper by studying the low-frequency spectral response of $BaTiO_3$ in the cubic and tetragonal phase, and $KNbO_3$ in the orthorhombic phase. Additionally, the model has been tested in this paper by studying KTN in the cubic and tetragonal phase. In all cases, it is successful at qualitatively explaining the symmetry properties and thermal behavior of the observed light scattering spectra. The model also quantitatively explains the thermal behavior of the width of the central peak seen above T_{c1} in KTN. These results are consistent with data taken using other methods that were noted in the introduction. For these reasons, the ES model should be considered an accurate representation of the low-frequency ionic dynamics in these crystals. Further tests of the applicability of the model to such crystals can be made by carrying out light scattering measurements (with an I_2 filter) in other phases that have not yet been studied, such as $KNbO_3$ in the cubic and tetragonal phase and $BaTiO_3$ or (high-Nb concentration) KTN samples in the orthorhombic phase. Finally, it should be noted that although these studies provide evidence for the existence of precursor clusters in cubic KTN, they do not yield any definite conclusions as to the origin of these clusters. This aspect of the problem merits further investigation.

ACKNOWLEDGMENTS

One of the authors (J.P.S.) was supported by National Science Foundation (NSF) Grant No. VMR-81-05005. The work at Lawrence Livermore National Laboratoiries (LLNL) was supported by the Division of Materials Sciences of the Office of Basic Energy Sciences, U.S. Department of Energy (DOE), and the LLNL under Contract No. W-7405-ENG-48. The work at Oak Ridge National Laboratory was supported by the Department of Materials Sciences, DOE, under Contract No. DE-AC05-84OR21400 with Martin Marietta Energy Systems, Inc.

[1]R. Comes, M. Lambert, and A. Guinier, C. R. Acad. Sci. Paris **226**, 959 (1968).

[2]G. Zaccai, A. W. Hewat, and K. D. Rouse, J. Phys. (Paris) Colloq. **33**, C2-133 (1972).

[3]G. Shirane, H. Danner, A. Pavlovic, and R. Pepinsky, Phys. Rev. **A3**, 672 (1954).

[4]Edward Lee, L. L. Chase, and L. A. Boatner, Phys. Rev. B **31**, 1438 (1985).

[5]L. L. Chase, J. Sokoloff, and L. A. Boatner, Solid State Commun. **55**, 451 (1985).

[6]S. Rod, F. Borsa, and J. J. Van der Klink, Phys. Rev. B **38**, 2267 (1988).

[7]O. Hanskepetitpierre, E. A. Stern, and Y. Yacoby, J. Phys. (Paris) Colloq. **47**, C8-675 (1986).

[8]A. D. Bruce and R. A. Cowley, J. Phys. C **6**, 2422 (1973).
[9]R. Migoni, H. Bilz, and D. Bäuerle, Phys. Rev. Lett. **37**, 1155 (1975).
[10]R. Migoni, H. Bilz, and D. Bäuerle, in *Lattice Dynamics*, edited by M. Balkanski (Flammarion, Paris, 1978), p. 650.
[11]G. E. Kugel, M. D. Fontana, and W. Kress, Phys. Rev. B **35**, 813 (1987).
[12]H. Vogt, in *Proceedings of the International Conference on Nonlinear Optics, Ashford Castle, Ireland, 1988* (unpublished).
[13]H. Vogt, Phys. Rev. B **38**, 5699 (1988).
[14]J. P. Sokoloff, L. L. Chase, and D. Rytz, Phys. Rev. B **38**, 597 (1988).
[15]M. D. Fontana, A. Ridah, and G. E. Kugel, Phase Trans. **9**, 147 (1988).
[16]Godefroy Kugel, Hans Vogt, Winfried Kress, and Daniel Rytz, Phys. Rev. B **30**, 985 (1984).
[17]H. Vogt, M. D. Fontana, G. E. Kugel, and P. Günter, Phys. Rev. B **34**, 410 (1986).
[18]H. Vogt, J. A. Sanjurjo, and G. Rossbroich, Phys. Rev. B **26**, 5904 (1982).
[19]H. Presting, J. A. Sanjurjo, and H. Vogt, Phys. Rev. B **28**, 6097 (1983).
[20]Y. Yamada and G. Shirane, Phys. Rev. **177**, 848 (1969).
[21]Kuon Inoue and Shigeru Akimoto, Solid State Commun. **46**, 441 (1983).
[22]Y. Luspin, J. L. Servoin, and F. Gervais, J. Phys. C **13**, 3761 (1980).
[23]M. D. Fontana, G. Metrat, J. L. Servoin, and F. Gervais, J. Phys. C **16**, 483 (1984).
[24]H. Uwe, K. B. Lyons, H. L. Carter, and P. A. Fleury, Phys. Rev. B **33**, 6436 (1986).
[25]K. B. Lyons, P. A. Fleury, and D. Rytz, Phys. Rev. Lett. **57**, 2207 (1986).
[26]W. Kleeman, F. J. Schafer, and D. Rytz, Phys. Rev. Lett. **54**, 2038 (1985).
[27]J. J. Van der Klink, S. Rod, and A. Chatelain, Phys. Rev. B **33**, 2084 (1986).
[28]O. Hanskepetitpierre, E. A. Stern, and Y. Yacoby, Brookhaven National Laboratory, National Synchotron Light Source Annual report, 1985 (unpublished), p. 176.
[29]J. A. Krumhansl and J. R. Schrieffer, Phys. Rev. B **11**, 3535 (1975).
[30]S. Aubry, J. Chem. Phys. **64**, 3392 (1976).
[31]T. Schneider and E. Stoll, Phys. Rev. B **31**, 1254 (1976).
[32]V. I. Halperin and C. M. Varma, Phys. Rev. B **14**, 4030 (1976).
[33]R. L. Prater, L. L. Chase, and L. A. Boatner, Phys. Rev. B **23**, 221 (1981).
[34]G. A. Samara, Phys. Rev. Lett. **53**, 298 (1984).
[35]R. Comes, M. Lambert, and A. Guinier, Solid State Comm. **6**, 715 (1968).
[36]A. Scalabrin, S. P. S. Porto, H. Vargas, C. A. S. Lima, and L. C. M. Miranda, Solid State Comm. **24**, 291 (1977).